$Na_v1.4$ Deregulation in Dystrophic Skeletal Muscle Leads to Na^+ Overload and Enhanced Cell Death

Carole Hirn, George Shapovalov, Olivier Petermann, Emmanuelle Roulet, and Urs T. Ruegg

Laboratory of Pharmacology, Geneva-Lausanne School of Pharmaceutical Sciences, University of Geneva, CH 1211 Geneva 4, Switzerland

Duchenne muscular dystrophy (DMD) is a hereditary degenerative disease manifested by the absence of dystrophin, a structural, cytoskeletal protein, leading to muscle degeneration and early death through respiratory and cardiac muscle failure. Whereas the rise of cytosolic Ca^{2+} concentrations in muscles of *mdx* mouse, an animal model of DMD, has been extensively documented, little is known about the mechanisms causing alterations in Na^+ concentrations. Here we show that the skeletal muscle isoform of the voltage-gated sodium channel, $Na_v1.4$, which represents over 90% of voltage-gated sodium channels in muscle, plays an important role in development of abnormally high Na^+ concentrations found in muscle from *mdx* mice. The absence of dystrophin modifies the expression level and gating properties of $Na_v1.4$, leading to an increased Na^+ concentration under the sarcolemma. Moreover, the distribution of $Na_v1.4$ is altered in *mdx* muscle while maintaining the colocalization with one of the dystrophin-associated proteins, syntrophin α-1, thus suggesting that syntrophin is an important linker between dystrophin and $Na_v1.4$. Additionally, we show that these modifications of $Na_v1.4$ gating properties and increased Na^+ concentrations are strongly correlated with increased cell death in *mdx* fibers and that both cell death and Na^+ overload can be reversed by 3 nM tetrodotoxin, a specific $Na_v1.4$ blocker.

The Journal of General Physiology

Downloaded from http://rupress.org/jgp/article-pdf/132/2/199/1785739/jgp_200810024.pdf by guest on 09 February 2026

INTRODUCTION

Duchenne muscular dystrophy (DMD) is a degenerative X-linked muscle disease affecting 1 male out of 3,500 newborns, leading to death through respiratory or cardiac muscle failure at age 20 to 30, with no effective treatment at present. Mutations in the p21 region of the X chromosome lead to an absence of dystrophin, a 427-kD protein located beneath the plasma membrane, which is associated with the cytoskeleton via actin, and with the extracellular matrix via a dystrophin–glycoprotein complex (DGC) (Blake et al., 2002). Because of its key localization, dystrophin is thought to play multiple roles such as maintaining mechanical stability of the muscle architecture (Koenig et al., 1988) or regulating the function of sarcolemmal components, for example, cation channels (Fong et al., 1990). The mechanisms leading to increased muscle cell death are still unclear; however, it is generally accepted that an elevated cytosolic calcium concentration occurring when muscle is stretched is an important link between the absence of dystrophin and muscle degeneration (Gailly, 2002; Ruegg et al., 2002).

This increase in the Ca^{2+} concentration is not the only alteration in dystrophin-lacking cells. Thus, it has been shown that the intracellular sodium concentration ($[Na^+]_i$) is also elevated in skeletal muscle of *mdx* mice, an animal model of DMD (Dunn et al., 1993; Allen, 2004). Additionally, an increase in Na^+/K^+ ATPase activity has been reported in *mdx* mice, suggesting an impairment in Na^+ regulation (Dunn et al., 1995). It has also been shown that fibers from *mdx* muscle are more susceptible to stretch-induced damage and that there is an associated rise in $[Na^+]_i$, which could be attenuated by unspecific cation channel blocker Gd^{3+} (Yeung et al., 2003). Nonetheless, the cause of the increased $[Na^+]_i$ is still unknown.

Voltage-gated sodium channels (VGSCs) are transmembrane proteins responsible for propagating the action potentials along the muscle fibers and initiating contraction. VGSCs are composed of a pore-forming α-subunit and a smaller β-subunit (Catterall, 1988). Two isoforms have been described in muscle: $Na_v1.4$, the skeletal muscle isoform that represents >90% of VGSCs expressed in skeletal muscle, and $Na_v1.5$, the fetal or cardiac isoform.

$Na_v1.4$ is highly expressed at the endplate of skeletal muscle fibers, but its detailed localization in the extrajunctional sarcolemma has not been studied extensively. Both isoforms contain the consensus sequence SXV-COOH, which binds directly to the PDZ domain of α1-syntrophin (Gee et al., 1998), a cytoplasmic protein

C. Hirn and G. Shapovalov contributed equally to this paper.

Correspondence to Urs T. Ruegg: urs.ruegg@pharm.unige.ch

Abbreviations used in this paper: DGC, dystrophin–glycoprotein complex; DMD, Duchenne muscular dystrophy; FDB, flexor digitorum brevis; TTX, tetrodotoxin; VGSC, voltage-gated sodium channel.

The online version of this article contains supplemental material.

© 2008 Hirn et al. This article is distributed under the terms of an Attribution–Noncommercial–Share Alike–No Mirror Sites license for the first six months after the publication date (see http://www.jgp.org/misc/terms.shtml). After six months it is available under a Creative Commons License (Attribution–Noncommercial–Share Alike 3.0 Unported license, as dscribed at http://creativecommons.org/licenses/by-nc-sa/3.0/).

The Rockefeller University Press $30.00
J. Gen. Physiol. Vol. 132 No. 2 199–208
www.jgp.org/cgi/doi/10.1085/jgp.200810024

belonging to the DGC. The distribution of dystrophin and syntrophin at the sarcolemma remains controversial, although results favor costameric and intercostameric localization (Williams and Bloch, 1999a). Moreover, it has been shown that in the heart, DGC is required for the proper expression and function of the $Na_v1.5$ isoform (Gavillet et al., 2006). These observations prompted us to test whether the absence of dystrophin could alter the expression and function of $Na_v1.4$, and whether the changes can account for the increase in $[Na^+]_i$ (Dunn et al., 1993; Allen, 2004).

We found that the absence of dystrophin modifies the expression level, distribution, and gating properties of $Na_v1.4$ in skeletal muscle. At the measured resting membrane potential, changes in gating properties and inactivation threshold are sufficient to support an observed twofold higher level of Na^+ under the sarcolemma in *mdx* muscle. This $[Na^+]_i$ elevation likely contributes to an elevated rate of cell death in dystrophic muscle, and both these effects can be reversed by tetrodotoxin (TTX) treatment at concentrations that specifically block the $Na_v1.4$ channel.

MATERIALS AND METHODS

Animals

Male C57BL/6J (control) and *mdx*^{5cv} mice were age matched to be 12–16 wk old. Mice were killed by cervical dislocation. All the procedures involving animals were performed in compliance with the Swiss Federal Veterinary Office's guidelines, based on the Swiss Federal Law on Animal Welfare, and approved by the Cantonal Veterinary Office.

Fiber Dissociation and Survival Test

Flexor digitorum brevis (FDB) muscles were dissected from both hind feet of the mice. After extraction, both muscles were incubated in DMEM supplemented with glutamax (GIBCO BRL), 2 mg/ml of collagenase type I-A (Sigma-Aldrich C-2674), and 10 μg/ml ciproxine (Bayer) for 1 h at 37°C. They were then rinsed three times with DMEM-glutamax and were dissociated by passing them repeatedly through wide-mouthed fire-polished Pasteur pipettes of decreasing size in DMEM until single intact fibers were obtained. The dissociated fibers were plated on coverslips coated with 400 μg/ml Matrigel (Becton Dickinson). For survival tests 50–100 fibers per well were plated in Matrigel-coated 48-well plates and treated with TTX (Alexis) at various concentrations in DMEM-glutamax (2 wells by concentration). Fiber survival was quantified daily by performing a blind count of living fibers, as judged by shape and light refraction using phase contrast optics under an inverted microscope (Nikon). No spontaneous contractile activity was observed in cultures of dissociated and denervated fibers.

Immunostaining of Isolated Fibers and Confocal Imaging

Freshly isolated fibers plated on coverslips (Labtek) were fixed in 1.5% solution of formaldehyde in PBS, washed twice in cold PBS, and then permeabilized in 0.2% Triton X-100 in PBS. The samples were incubated in 10% normal goat serum in PBS followed by an overnight incubation at 4°C with the primary antibody (1:500 dilution) in PBS containing 0.05% Triton X-100. After extensive washing, fibers were incubated with a fluorophore-conjugated secondary antibody (1:500 dilution, Molecular Probes) in PBS for 1 h at room temperature. Finally slides were mounted in Mowiol (Calbiochem). $Na_v1.4$ was labeled using an anti-SkM1 mouse monoclonal antibody (Sigma-Aldrich S9568) and α1 syntrophins with an anti-α1-syntrophin rabbit polyclonal antibody (provided by M. Schaub, University of Zurich, Zurich, Switzerland). Secondary antibodies were AlexaFluor 488–labeled monoclonal goat anti-rabbit, and Texas red–labeled monoclonal goat anti-mouse.

Confocal images were obtained using a Leica SP2 confocal microscope with a 40× oil immersed objective with 1.4 numerical aperture. The pixel dimensions were 0.2 × 0.2 μm in the focal plane, and the z sections were 0.1–0.4 μm. The same settings were used for all images. Slides were excited at either 488 or 594 nm depending on the secondary antibody.

Western Blots

FDB muscles were homogenized in a buffer containing (in mM) 20 HEPES, pH 7.6, 125 NaCl, 1 EDTA, 1 EGTA, 1 DTT, 10% glycerol, protease inhibitor cocktail using an Ultra-Turrax T8 homogenizer (Verrerie de Carouge). Triton-X was added to a final concentration of 1% and homogenates were incubated 10 min on ice. After centrifugation (12,000 *g*, 4°C, 20 min), supernatants were collected. Protein concentration was determined using the BC assay method (Optima). 5 μg of protein were resolved on a gradient gel (5–10% of acrylamide) at 80 V. Proteins were transferred onto 0.45-μm nitrocellulose membranes for 2 h at 100 V at 4°C (Bio-Rad Laboratories Inc. Miniprotean III apparatus). Transfer efficiency was verified by staining with Ponceau S (Sigma-Aldrich).

Membranes were blocked in saturation solution (TBST containing 3% BSA) for 1 h and incubated overnight at 4°C with a primary antibody (anti-SkM1, Sigma S-9568, 1:5,000) in saturation solution. After extensive washing, membranes were exposed to secondary antibodies (HRP-conjugated goat anti-mouse antibody, Bio-Rad Laboratories Inc., 1:50,000) for 1 h. Proteins were detected by chemiluminescence using the ECL plus kit (Amersham Biosciences) on Fuji x-ray film, and were quantified using the Bio-Rad Laboratories Inc. scanner (Universal Hood II, Quantity one analysis software) and normalized to expression level of SERCA1. Western blot analysis of SERCA1 expression was performed using mouse anti-SERCA1 antibody (Affinity Bioreagents 1:1,000). Expression of SERCA1 has been shown to be essentially the same in FDB muscles from C57BL/6J and *mdx*^{5cv} mice (Boittin et al., 2006).

Measurement of Sodium Influx in FBD Muscle

FDB muscles were rinsed in PBS, incubated with 1 μCi of $^{22}Na^+$ in PSS (in mM: HEPES 5, KCl 5, $MgCl_2$ 1, NaCl 145, $CaCl_2$ 1.2; pH 7.3) in the presence of 10^{-4} M ouabain (Merck) in order to inhibit Na^+/K^+ATPase activity, with or without 3×10^{-9} M TTX. No preincubation was performed and muscles were incubated for 5 min, rinsed four times in ice-cold PSS with ouabain, soaked, weighed, and extracted overnight with 3 N NaOH. $^{22}Na^+$ content was determined by liquid scintillation counting using a β-counter (LKB Wallac) normalized by dividing by muscle weight and expressed as ratio of nontreated control muscle.

Patch Clamp Recordings

Cell-attached patch-clamp recordings were performed at room temperature on individual fibers isolated as described above. Fibers were immersed in a relaxing, high K solution (in mM: 10 NaCl, 142 KCl, 2 $MgCl_2$, 0.2 $CaCl_2$, 5 glucose, 0.5 EGTA, 10 HEPES; pH 7.3) containing additionally 30 μM *N*-benzyl-p-toluene sulphonamide (BTS) to inhibit contractions. Cells immersed in this solution had their resting membrane potentials within 2 mV of zero. Patch pipettes contained a Tyrode solution (in mM: 140 NaCl, 5 KCl, 0.5 $MgCl_2$, 1 $CaCl_2$, 6 glucose, 10 HEPES; pH 7.3) with 2 mM TEA and 10 μM 4,4'-diisothiocyanato-stilbene-2,2'-disulphonic acid (DIDS) added to inhibit K^+ and Cl^- currents. Resting membrane potential measurements were performed in control and *mdx* fibers immersed in the physiological Tyrode solution

Downloaded from http://rupress.org/jgp/article-pdf/132/2/199/1785739/jgp_200810024.pdf by guest on 09 February 2026

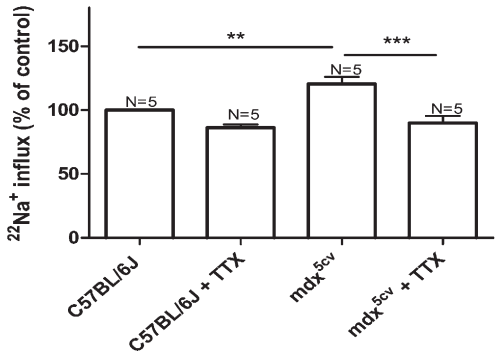

Figure 1. TTX blocks enhanced basal sodium influx in *mdx*^{5cv} FDB muscle. Isolated muscles were incubated for 5 min in the presence of $^{22}Na^+$ with or without 3×10^{-9} M TTX. After extensive washing, muscle tissue–associated radioactivity was quantified by scintillation counting. Influx in *mdx*^{5cv} muscles and inhibition of influx by TTX is expressed as percentage of influx in the non-treated control (C57BL/6J) muscle (ANOVA: **, $P < 0.01$; ***, $P < 0.001$). Values are reported as means ± SEM.

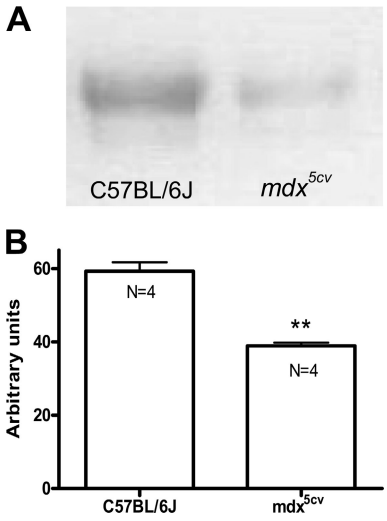

Figure 2. $Na_v1.4$ expression levels in *mdx* and C57BL/6J FDB muscles. (A) Representative Western blot analysis of $Na_v1.4$ channels from *FDB* muscle extracts of control C57BL/6J and *mdx*^{5cv} mice. Each slot represents the extract from one *FDB* muscle of one 12–16-wk-old mouse. (B) Quantification of $Na_v1.4$ expression levels (four mice/group). Protein concentrations were measured in triplicate to guarantee equal loading, and $Na_v1.4$ density is expressed in arbitrary units using SERCA1 as an internal control (**, $P < 0.01$; Student's unpaired *t* test). Values are reported as means ± SEM.

with sharp pipettes filled with 3 M KCl. Pipettes were pulled using the horizontal puller P2000 (Sutter Instrument) and had a resistance consistently lying in the range of 4–6 MOhm for patch pipettes and 6–7 MOhm for sharp electrodes. Electric currents were acquired and low-pass filtered at 10 kHz with a HEKA EPC-7 amplifier (HEKA Elektronik), and then digitized with a Digidata 1322 digitizer (Molecular Devices) at 100 kHz. Patch-clamp currents were normalized per the area of the patch by multiplying currents by the resistance of the corresponding pipette and then dividing by the average pipette resistance.

Stimulation protocols used to study activation and inactivation properties of VGSCs are shown on the insets of Fig. 3 B and Fig. 4 A. In short, patches were held at −100 mV between stimulation applications. The inactivation-recovery prepulses to −120 mV were applied for 30 ms and then potential was stepped up to voltages ranging from −70 to +40 mV or, during the determination of Na^+ reversal potential, to +100 mV in steps of 10 mV for 20 ms. To study inactivation properties, the patches were held for 500 ms at voltages ranging from −120 to −10 mV in steps of 10 mV and currents were sampled at 10 mV for 50 ms. For the purpose of leak subtraction, the stimulation protocols were extended by a 20-ms step from the holding potential of −100 mV to −80 mV. Additionally, after performing recordings as described, currents were acquired using the online leak subtraction as implemented in Clampex program (pClamp-9 suite, Axon Instruments). Both methods allowed equivalently good removal of leakage currents during the study of activation properties of Nav1.4 channels. Only online leak subtraction was used to study the inactivation properties of these channels.

Individual responses at every sampling potential were extracted and fit with the Hodgkin-Huxley model with the help of custom made software, which can be downloaded at http://www.unige.ch/sciences/pharm/fagie/software/elphys_utils-20080407.tar.bz2. Fit convergence was verified by recalculating the peak currents from the obtained fit parameters and comparing them with the apparent peak currents, as well as by fitting only tail regions of VGSC responses using Clampfit 9 software (pClamp-9 suite) and comparing the resulting inactivation rates (τ_i). Averages were computed by first calculating per patch means of the corresponding individual values and then establishing the overall averages. Typically, three recordings were performed for every patch. Patches where a significant rundown of signal or nonspecific activity was detected were discarded. Reversal potential for Na^+ was determined by fitting tails of individual IV curves in the region where the tails were linear (typically 10–30 or, for patches with large currents, 40 mV) and averaging the calculated intersections with I = 0 first per patch and then for all patches. These data analyses were supplemented by traces with the sampling voltage steps extended to 100 mV, in order to perform control measurements of zero-current crossings. Details of these data analyses can be found in online supplemental material. Statistical modeling and composition of histograms (Fig. 5 B) were performed with the help of the R project for statistical computing (http://www.r-project.org/). Plots of sample $Na_v1.4$ traces, steady-state activation and inactivation curves, and fit parameters were prepared using Microcal Origin software (Origin Laboratory).

Online Supplemental Material

The online supplemental material (available at http://www.jgp.org/cgi/content/full/jgp.200810024/DC1) contains the detailed description of data analyses performed in order to reliably measure Na^+ reversal potential, including Fig. S1.

RESULTS

Sodium Influx through $Na_v1.4$ Is Increased in *mdx* Muscle

To investigate whether Na^+ influx through voltage-gated Na^+ channels was altered in dystrophin-deficient muscle, we studied the global Na^+ influx using $^{22}Na^+$ as a tracer. The observed basal Na^+ influx in C57BL/6J FDB muscle was 31.5 ± 4.4 cpm/mg and was taken as 100%. As can be seen in Fig. 1, Na^+ influx increased by 20 ± 5.6% ($P = 0.003$) in *mdx*^{5cv} muscles compared with that of control FDB muscles. Similar increases associated with dystrophin deficiency were found in EDL and SOL muscles (unpublished data). We then tested whether the basal

Downloaded from http://rupress.org/jgp/article-pdf/132/2/199/1785739/jgp_200810024.pdf by guest on 09 February 2026

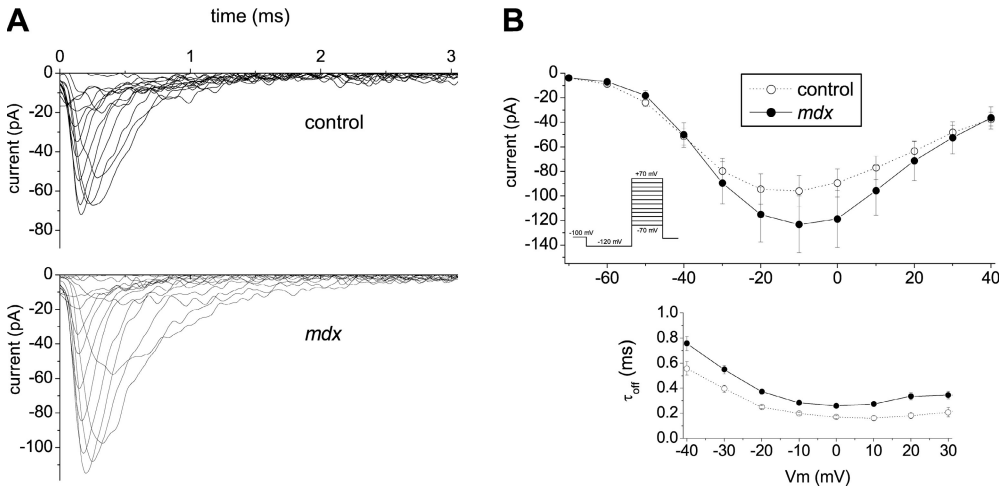

Figure 3. Electrophysiological measurements of $Na_v1.4$ activity in cell-attached patches. (A) Representative traces of cell-attached Na^+ currents in C57BL/6J (top) and *mdx*^{5cv} (bottom) FDB fibers. Of note are the longer inactivation tails in *mdx*^{5cv} traces. Currents were elicited with an activation protocol shown on the inset of B. (B) Comparison of average currents (top) and inactivation time constants τ_i (bottom) for the control (open circles, 28 patches) and *mdx* (filled circles, 33 patches) recordings. Inactivation time constants for potentials below −40 and above 30 mV could not be reliably estimated because of small current amplitude and are not shown. Values are reported as means ± SEM.

Na^+ influx measured in control and dystrophic muscles was affected by TTX, a high-affinity inhibitor of $Na_v1.4$ channels (Ritchie and Rogart, 1977). Whereas TTX at a concentration of 3×10^{-9} M had no significant effect on control muscles, it produced a significant reduction of Na^+ entry in *mdx*^{5cv} muscles (30%, Fig. 1). TTX treatment restored Na^+ influx into *mdx*^{5cv} fibers to a level indistinguishable from that of C57BL/6J muscles, suggesting that $Na_v1.4$ channels play an important role in regulating $[Na^+]$ under the sarcolemma of *mdx* muscles.

Expression of $Na_v1.4$ Is Decreased in *mdx* FDB Muscle

To investigate whether the increased sodium entry observed in *mdx*^{5cv} cells is caused by overexpression of $Na_v1.4$ channels, we performed Western blot and real time PCR analyses. Protein concentrations were measured in triplicates to guarantee equal loading. $Na_v1.4$ density was expressed in arbitrary units using SERCA1 as an internal control (Boittin et al., 2006). Surprisingly, $Na_v1.4$ protein levels were 35% smaller in *mdx*^{5cv} than in control muscles (Fig. 2, A and B). We and others (Ribaux et al., 2001) obtained similar results with EDL muscle where $Na_v1.4$ expression was decreased by 40% in *mdx*^{5cv} compared with control muscle (unpublished data). Thus, $Na_v1.4$ channels are underexpressed, rather than overexpressed, in *mdx* fibers, highlighting the importance of a proper explanation of the increased Na^+ entry.

Sodium Current Is Observed at Similar Levels in Control and *mdx* Fibers

To determine whether the increase in $[Na^+]_i$ observed in *mdx*^{5cv} fibers is caused by changes in kinetic properties of Na^+ channels, we performed patch-clamp measurements. To avoid possible changes in the expression levels of $Na_v1.4$ channels following fiber isolation, measurements were performed within a few hours after harvesting the cells.

Fig. 3 A shows typical Na^+ currents induced in FDB fibers using the protocol displayed on the inset of Fig. 3 B. Patches were held at −100 mV between stimulation applications. The inactivation-recovery prepulses to −120 mV were applied for 30 ms and then potential was stepped up to voltages ranging from −70 to +40 mV in steps of 10 mV for 20 ms. The addition of 50 nM TTX to the pipette solution blocked this activity completely (unpublished data), confirming prevalence of the skeletal muscle isoform in these fibers, namely $Na_v1.4$. Current–voltage relationships are shown in Fig. 3 B, top panel. While average currents suggest an increased Na^+ entry in *mdx*^{5cv} fibers, this difference was not significant.

$Na_v1.4$ Channels Inactivate Slower in *mdx* Fibers

To assess kinetic properties of Na^+ channels we fit individual traces with the Hodgkin-Huxley model (Hodgkin and Huxley, 1952) determining the amplitude parameter *A*, corresponding to the density of the channels in the patch and activation/inactivation time constants τ_{on} and τ_i. The fit parameters of individual traces thus obtained were used to recalculate current at the peak and compare it with the apparent value for the trace, as a means of controlling fit convergence. Additionally, tails of randomly selected traces were fit with exponential dependence and the resulting time constants were compared with the corresponding τ_i's of the model fits. Fitting the traces with the Hodgkin-Huxley model yielded good convergence for the traces exhibiting maximum peak currents >10 pA. Patches with maximum peak current <10 pA did not show good fit convergence and were considered empty (3 of 31 or ∼10% C57BL/6J and 9 of 42 or ∼20% *mdx*^{5cv}).

Downloaded from http://rupress.org/jgp/article-pdf/132/2/199/1785739/jgp_200810024.pdf by guest on 09 February 2026

Data analysis yielded amplitude parameters *A* of 284 ± 50 pA for control and 216 ± 34 pA for *mdx*^{5cv} fibers. As with average currents, average amplitudes suggest a possible, but not significant, difference in the expression levels of $Na_v1.4$ channels. Peculiarly, while average currents tended to be larger, the average amplitudes hint at a smaller expression level of $Na_v1.4$ in *mdx*^{5cv} as compared with C57BL/6J fibers.

These observations were complemented by a significant increase of inactivation time constants (τ_i). While values obtained for control fibers corresponded to those reported (Ulbricht, 2005), the τ_i's of *mdx*^{5cv} fibers were ~1.5 times larger (Fig. 3 B, bottom). This increase in open dwell times causes an increased entry of Na^+ into the cells and allows reconciling the inverse signs of change in observed currents and estimated amplitudes. Activation time constants of the currents were typically in the 0.1–0.2 ms range, corresponding to the resolution attainable at the used bandwidth of 10 kHz. Therefore, no conclusion could be drawn as to whether τ_{on} values in control fibers differ from those of *mdx*^{5cv} fibers.

$Na_v1.4$ Channels Inactivate at Less Negative Potentials in *mdx* Fibers

Representative steady-state activation and inactivation curves are shown in Fig. 4 A, using the stimulation protocols shown in the insets of Fig. 3 B and Fig. 4 A. To sample inactivation properties, the patches were held at voltages ranging from −120 to −10 mV and were changed in steps of 10 mV for 500 ms and currents were sampled for 50 ms. Individual curves were fit with the Boltzmann function, and the transition thresholds were first averaged per patch before overall averages were produced. The thresholds of steady-state activation did not differ significantly (−33.8 ± 1.5 mV for control and −29.6 ± 2 mV for *mdx*^{5cv} fibers). On the other hand, steady-state inactivation thresholds were shifted by ~10 mV toward more positive potentials for *mdx*^{5cv} in comparison with those of control fibers (−89.4 mV ± 2 mV for control and −79.5 mV ± 2.5 mV for *mdx*^{5cv} fibers, P = 0.01).

To investigate the effect of this shift, resting membrane potentials (V_{rest}) of the fibers were determined with sharp electrodes filled with 3 M KCl. Resting membrane potentials were measured in I = 0 mode, yielding −49.7 ± 1.5 mV in control and −50.8 ± 1.6 mV in *mdx* fibers (mean ± SEM). Fig. 4 B shows window currents calculated for the above average activation and inactivation curve parameters for control (dashed line) and *mdx* (solid line) fibers with a vertical dashed line marking the measured V_{rest} position. As can be seen, at such V_{rest} one can expect an approximately twofold higher probability of $Na_v1.4$ opening in *mdx* as compared with control cells.

$[Na^+]$ under the Sarcolemma Is Elevated in *mdx* Fibers

To assess how these changes in $Na_v1.4$ gating properties influence $[Na^+]$ under the sarcolemma, we measured

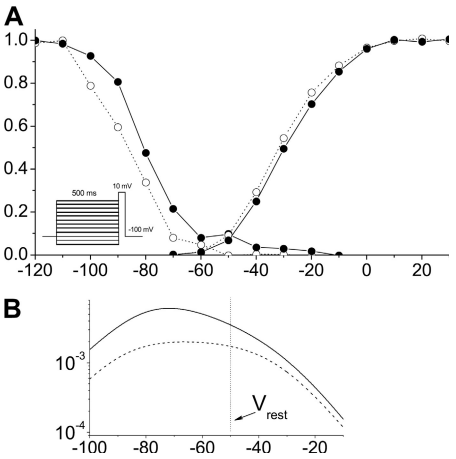

Figure 4. Steady-state activation and inactivation. (A) Representative steady-state activation and inactivation curves. Individual curves were fit with the Boltzmann function, and midpoints were averaged per patch and then overall averages were calculated, yielding no significant differences between activation thresholds (−33.8 ± 1.5 mV for control and −29.6 ± 2 mV for *mdx*^{5cv}patches). However, a shift of ~10 mV toward more positive potentials for inactivation thresholds was observed in *mdx*^{5cv} (−89.4 mV ± 2 mV for control and −79.5 mV ± 2.5 mV for the *mdx*^{5cv} fibers, P = 0.01). The stimulation protocol used to produce currents for the inactivation curves is shown on the inset. (B) Window currents calculated from the determined average activation/inactivation thresholds and slopes at midpoint. Vertical line at −50 mV represents measured resting membrane potential, emphasizing an ~2× increase in opening probability of $Na_v1.4$ channels at rest in *mdx* fibers.

the reversal potential for Na^+. Tail regions of current–voltage relations (typically 10–30 mV or, for the traces with larger currents, 40 mV) were fit with linear dependence and the intersections with the I = 0 line were determined and averaged for *mdx* and control cells as described, yielding 69.9 ± 5 mV for control and 51.7 ± 5 mV for *mdx* fibers (28 and 33 patches correspondingly, IV curves generated as described in previous subsections were used). To control the representativity of such fits we extended the activation protocol (Fig. 3 B, inset) to apply sampling voltage steps of as much as 100 mV, with the intention of directly observing the reversal of the Na^+ current. Unfortunately application of large voltages made patches unstable, significantly decreasing the proportion of surviving patches. Additionally, small overall currents caused large distortions in the derived IV curves in the zero-crossing region (40–100 mV), yielding results with a significant margin of systematic error (see online supplemental material for a detailed description, available at http://www.jgp.org/cgi/content/full/jgp.200810024/DC1) which, however, agree with the reversal potentials derived by fitting stable tail regions, as described above, at 67.8 ± 6 mV for control (five patches) and 52.7 ± 5 mV for *mdx* fibers (six patches), yielding overall averages of 69.6 ± 5 mV for control and 52.5 ± 5 mV for *mdx* (mean ± SEM, P = 0.02).

Downloaded from http://rupress.org/jgp/article-pdf/132/2/199/1785739/jgp_200810024.pdf by guest on 09 February 2026

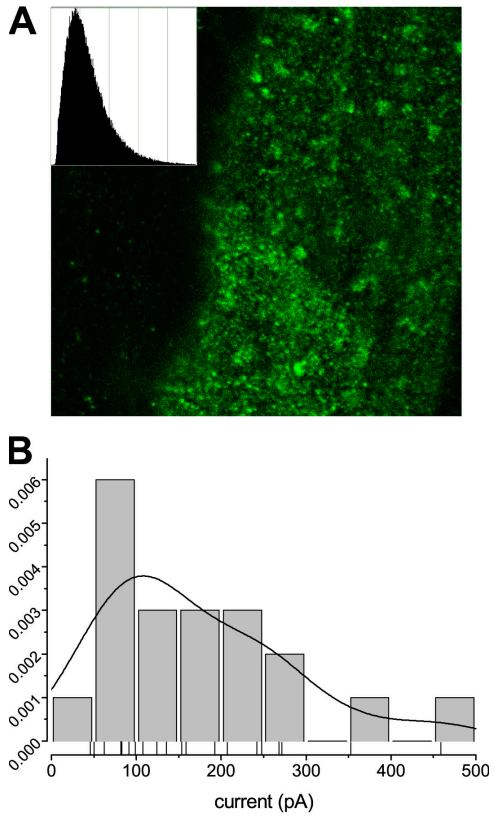

Figure 5. $Na_v1.4$ channel clusters in sarcolemma of control and *mdx* fibers. (A) Confocal images of $Na_v1.4$ localization. Isolated fibers were immunolabeled with mouse antibodies to $Na_v1.4$. A fluorescent signal was observed primarily at the sarcolemma. The luminescence distribution plot (inset) shows nonuniform density corresponding to apparent clusters of Na^+ channels. (B) Distribution of $Na_v1.4$ expression levels in cell-attached patches (model parameter *A* in fits with the Hodgkin-Huxley model) displays a similar non-Gaussian shape corresponding to that observed in confocal microscopy. The continuous curve represents the distribution density of amplitudes calculated using a Gaussian kernel density estimate with the bandwidth of 40 pA from the data points plotted below the histogram as thin vertical lines.

At the conditions under which the recordings were performed (TEA and DIDS in the pipette, traces with nonspecific activity discarded), only the Na^+ currents could be observed, allowing us to use the Nernst equation in order to derive the $[Na^+]$ under the sarcolemma. The calculations were done for the individual traces and then calculated concentrations were averaged to produce overall $[Na^+]$ levels, yielding 9.3 ± 2 mM for control C57BL/6J fibers and 18.1 ± 4 mM for mdx^{5cv} fibers.

$Na_v1.4$ Channels Cluster in Sarcolemma of Control and *mdx* Fibers

One peculiar feature observed during patch clamp recording was an unusually high variability of Na^+ currents recorded in the patches. Differences of 40 pA in current and almost 70 pA in amplitude (an ~30% difference, fit parameter *A* above) were made insignificant because of patch-to-patch variability. On the other hand, the τ_i's were very consistent and significantly differed between control and mdx^{5cv} fibers.

To investigate whether such variability was caused by ion channel clustering in the plasma membrane, we immunolabeled mdx^{5cv} and C57BL/6J fibers with monoclonal anti-SkM1 antibody and performed confocal imaging of labeled fibers. Fig. 5 A shows the confocal image of part of the mdx^{5cv} fiber sarcolemma, with the inset showing luminescence distribution in the part containing the membrane. The distribution was not simply Gaussian, as one would expect in case of diffuse distribution of ion channels in the plasma membrane; instead it had a characteristic tail, corresponding to hot spots representing clusters of the channels apparent on the image. Fig. 5 B shows the distribution of amplitude parameters, representative of channel expression density at the point of patch formation, calculated from Hodgkin-Huxley fits to the currents in cell-attached patches made to the mdx^{5cv} fibers as described above. A similar tail, emphasizing the asymmetrical presence of amplitudes larger than the value of the main peak, can be observed in this panel. Control fibers yielded a similar distribution of amplitude parameter densities, thus confirming the hypothesis that $Na_v1.4$ channels cluster in the sarcolemma of muscle fibers.

Distribution Pattern of $Na_v1.4$ Is Altered in Isolated *mdx* Fibers

To further investigate the distribution of VGSCs, and to test whether the absence of dystrophin influences Na^+ channel gating properties via syntrophin, we performed confocal imaging of mdx^{5cv} and control fibers labeled with an anti-SkM1 monoclonal antibody against $Na_v1.4$, and a polyclonal antiserum against α1-syntrophin, as described above.

Confocal images captured at the surface of the cells revealed an intense signal at the muscle endplate, as assessed by fluorescently labeled α-bungarotoxin (not depicted), and on the surface of the fiber, dispersed over the area of the fiber (Fig. 6 A). By contrast, in the confocal planes crossing the cells, labeling was localized to the sarcolemma, with only a background level of fluorescence in the cytoplasm (Fig. 6 B). No fluorescence was detected when primary antibodies were omitted (not depicted).

Fibers from C57BL/6J muscle showed a longitudinally striated pattern (Fig. 6 C); 53 out of 63 fibers exhibited a pattern parallel to the longitudinal axis of the fibers reminiscent of the L-domain of costamers (Bloch et al., 2002). Interestingly, this pattern was present in only 16 out of 57 mdx^{5cv} fibers. The majority of fibers showed a disorganized labeling (Fig. 6 C), suggesting that, at the sarcolemma of mdx^{5cv} fibers, $Na_v1.4$ channel distribution is altered by the absence of dystrophin and undergoes a change in organization as described for other

Downloaded from http://rupress.org/jgp/article-pdf/132/2/199/1785739/jgp_200810024.pdf by guest on 09 February 2026

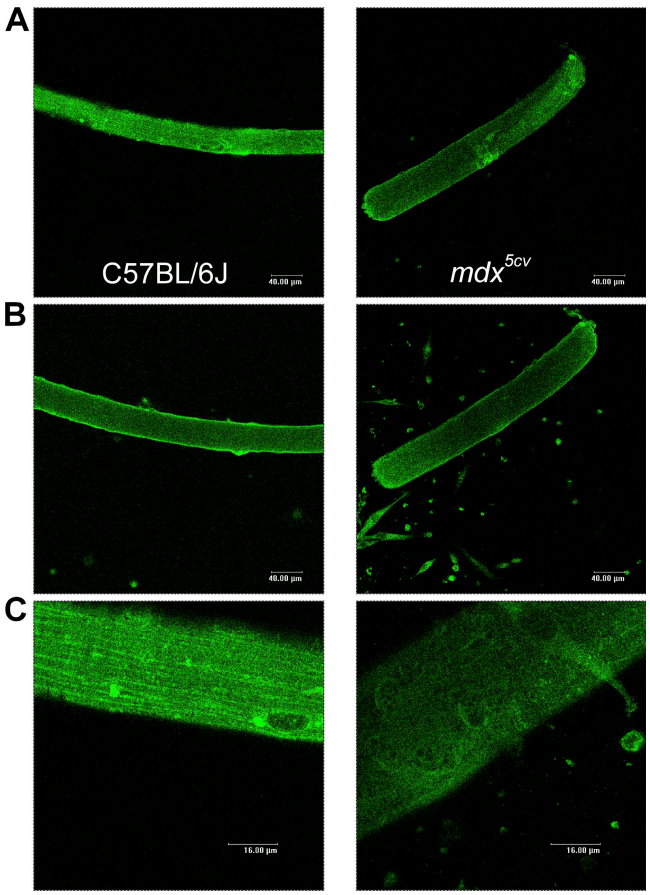

Figure 6. Distribution pattern of $Na_v1.4$ is altered in *mdx* fibers. $Na_v1.4$ channel distribution in isolated FDB fibers; comparison between C57BL/6J and mdx^{5cv} (four mice each condition). $Na_v1.4$ immunofluorescence (green) in single C57BL/6J fibers (left) and mdx^{5cv} fibers (right) captured at the surface (A) or in deeper part of the cells (B). (C) 4× zoom of A.

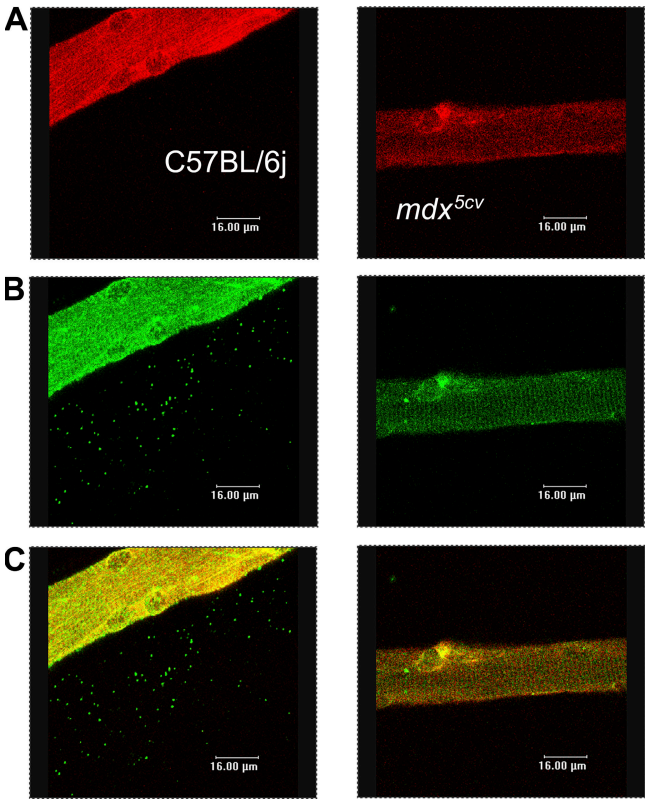

Figure 7. $Na_v1.4$ colocalizes with α1-syntrophin. High magnification views of C57BL/6J fibers (left) and mdx^{5cv} fibers (right). Coimmunolabeling of $Na_v1.4$ (A) and α1-syntrophin (B) in C57BL/6J fibers and mdx^{5cv} fibers. (C) Merged fluorescence.

plasma membrane–associated proteins. Additionally, in good agreement with the results obtained by Western blot analysis, we observed a decrease in $Na_v1.4$ channel density in mdx^{5cv} as compared with control fibers (Fig. 6 C).

To investigate the localization of the $Na_v1.4$, we coimmunolabeled it with α1-syntrophin, the main syntrophin expressed in muscle. We observed a reduced expression of this syntrophin in mdx^{5cv} muscle (Fig. 7 B), similar to what was reported by Williams and Bloch (1999b). As expected, $Na_v1.4$ colocalized quite well with α1-syntrophin at the sarcolemma in both types of muscle (Fig. 7 C), repeating a costameric pattern similar to that of $Na_v1.4$ channels, strongly suggesting that syntrophins are an important link between $Na_v1.4$ and dystrophin, whose absence leads to alterations in distribution patterns of both proteins studied here.

Tetrodotoxin Increases Survival of Isolated *mdx* Fibers

To determine the involvement of VGSCs in mdx^{5cv} muscle cell death we investigated the effect of tetrodotoxin on survival of isolated fibers. As shown in Fig. 8 A, the percentage of living C57BL/6J and mdx^{5cv} fibers in culture decreased with time, however at a faster rate in the case of *mdx* cells. For the first 3 d in culture ∼25% less mdx^{5cv} fibers survived than C57BL/6J ones.

Furthermore, we assessed the effect of TTX on fiber survival (Fig. 8, B and C). Two concentrations of TTX (3×10^{-9} and 10^{-8} M) that specifically inhibit $Na_v1.4$, but not $Na_v1.5$, channels (Ritchie and Rogart, 1977) were tested and yielded identical results. We observed no significant effect on C57BL/6J survival (Fig. 8 B); however, TTX significantly improved survival of mdx^{5cv} fibers in culture, bringing the survival rate close to that of control fibers (Fig. 8 C). On the other hand, the sub-IC_{50} concentration of TTX (10^{-9} M) did not have any significant effect.

DISCUSSION

Dystrophic muscle fibers from humans or mice have been shown to have an elevated concentration of Na^+ under their sarcolemma (Dunn et al., 1993; Constantinides et al., 2000; Allen, 2004). However, the mechanisms involved in this elevation have not been investigated so far. We report here that deregulation of $Na_v1.4$, the VGSC isoform that accounts for the bulk of Na^+ channels expressed in the sarcolemma of skeletal muscle,

Downloaded from http://rupress.org/jgp/article-pdf/132/2/199/1785739/jgp_200810024.pdf by guest on 09 February 2026

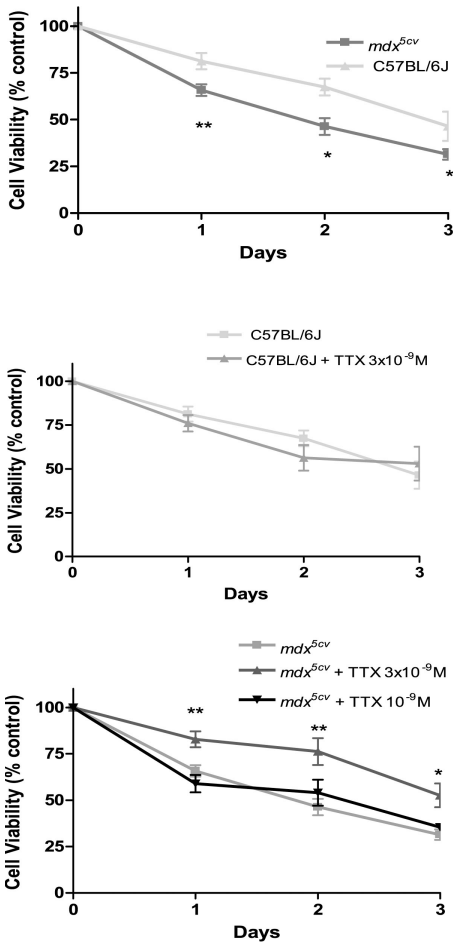

Figure 8. Tetrodotoxin improves survival of isolated *mdx* fibers. Isolated fibers were plated on 24-mm diameter Matrigel-coated culture dishes and left for 4 h at 37°C. Afterwards buffer was added with or without TTX (3×10^{-9} M) and the numbers of living cells were immediately determined. Time 0 is taken as 100%. (A) Comparison between C57BL/6J ($n = 5$) and mdx^{5cv} ($n = 5$) fibers surviving at 0, 1, 2, and 3 d after addition of the buffer. Effect of 3×10^{-9} M TTX on C57BL/6J (B) and mdx^{5cv} (C) fiber survival (Student's unpaired *t* test: *, $P < 0.05$; **, $P < 0.01$). Values are reported as means ± SEM.

significantly affects Na^+ influx in *mdx* muscle fibers and can, at least partially, explain this increased $[Na^+]_i$. While increased Na^+ entry in stimulated *mdx* muscle, in association with up-regulated activity of stretch-activated channels has been known (Yeung et al., 2003; Allen, 2004), the alteration of $Na_v1.4$ gating properties reported in this paper appears to be important for both basal and stimulated Na^+ entry and likely plays no less important a role in causing excessive Na^+ entry in *mdx* muscle fibers.

We observed that Na^+ entry in dystrophic fibers, as assessed by $^{22}Na^+$ uptake, was increased by 20% over that of control fibers. Incubating the cells with a concentration of TTX that specifically blocks the skeletal ($Na_v1.4$), but not the cardiac ($Na_v1.5$), isoform (Goldin, 2001) produced no significant effect on control fibers, while it reduced the influx in mdx^{5cv} muscle to the control level. In agreement with this, fiber survival was significantly worsened in the case of mdx^{5cv} cells, but could also be restored to the levels observed in control fibers by application of TTX (Fig. 8 C). Taking into account that currents in cell-attached patches were completely blocked by TTX, we confirm that Nav1.4 is the primary isoform expressed in the sarcolemma of both dystrophic and control fibers and that the up-regulated activity of $Na_v1.4$ channels is primarily responsible for the increase in Na^+ influx in dystrophin-deficient muscle cells, significantly affecting their survival.

Similar effect of TTX has been reported in neurons, where it reduced neuronal death and blocked Na^+ entry during hypoxia, improving survival of cultured neocortical neurons (Banasiak et al., 2004). In that case, TTX attenuated apoptotic neuronal death via a reduction in caspase-3 activation. Moreover, veratridine, a stimulator of VGSC activity, induced Na^+ overload, leading to increased cell death (Koike et al., 2000). Thus, it can be argued that maintaining a proper Na^+ balance is important for optimal muscle survival and function. In particular, Na^+ overload in mdx^{5cv} fibers significantly contributes to cell degradation and early death.

One possible explanation for the increase in Na^+ influx is that it is caused by overexpression of $Na_v1.4$ in *mdx* muscles. However, our Western blot measurements, as well as estimates of expression levels of $Na_v1.4$ channels in patch pipettes together with a higher incidence of empty patches showed that this was not the case. Furthermore, we investigated whether the distribution of Na^+ channels in the sarcolemma was disturbed in dystrophin-deficient cells. Analysis using confocal imaging of isolated FDB fibers allowed an accurate localization of the protein. Channels were observed exclusively at the membrane and showed an unusual longitudinally oriented pattern likely corresponding to the longitudinal (L) domains oriented in parallel to the long axis of the muscle fiber (Bloch et al., 2002). These L domains, while present universally in normal fibers, were often distorted in *mdx* myofibers due to disorganized costamers. It seems that $Na_v1.4$ protein is directly attached to an L domain in normal muscle, and the absence of dystrophin leads to irregularities in its anchorage, implying that the DGC is required for proper localization and function of the VGSCs.

Interestingly, $Na_v1.4$ in our experiments with skeletal muscle colocalized with syntrophin, similarly to what has been described for the cardiac isoform $Na_v1.5$ (Gee et al., 1998; Gavillet et al., 2006). Syntrophins are costameric proteins known to interact directly with both types of muscle VGSCs, however they also show an intercostameric pattern, responsible for the longitudinal strands (Williams and Bloch, 1999a,b). In *mdx* muscle their expression is lower than in control muscle and their distribution shows a broad range of disrupted patterns,

Downloaded from http://rupress.org/jgp/article-pdf/132/2/199/1785739/jgp_200810024.pdf by guest on 09 February 2026

similarly to what we observed for $Na_v1.4$ (Bloch et al., 2002). Moreover Gee and coworkers observed, in vitro, that the C-terminal biotinylated peptide of $Na_v1.4$ binds syntrophin via its PDZ domain (Gee et al., 1998). Taken together with our observations this suggests that α1-syntrophin is the main link between dystrophin and $Na_v1.4$. and that dystrophin deficiency leads to disruption of distribution of both of these proteins. Work is in progress to assess the role and the distribution of $Na_v1.5$, as well as the interaction of β1 and β2 syntrophins with $Na_v1.4$ in dystrophin-deficient muscle cells.

The observation of an altered distribution pattern of $Na_v1.4$ channels in *mdx*^{5cv} fibers, which in itself involves important considerations, cannot fully explain the increase in Na^+ influx in view of the smaller amount of the protein in sarcolemma. To resolve this ambiguity we turned to patch-clamp measurements of Na^+ currents to study how the gating properties of $Na_v1.4$ are modified in dystrophin-deficient cells. Unfortunately, differences in overall currents and amplitude parameters, while not small, were masked by the high patch to patch variability due to nonuniform distribution of channels. Nonetheless it is interesting to note that mean currents were larger in *mdx*^{5cv} fibers while amplitudes, representing the expression level of $Na_v1.4$, were smaller. On the other hand, the finding that inactivation times were consistently and by a big margin larger in *mdx*^{5cv} cells enables to explain the increased stimulated inward Na^+ current in spite of the decreased $Na_v1.4$ expression levels.

Another important observation, producing even more significant effect on basal Na^+ entry, is the shift of the inactivation threshold by ∼10 mV toward less negative potentials. While resting membrane potentials were not affected by the absence of dystrophin, the shift in the inactivation curve itself is sufficient to cause an approximately twofold higher activity of $Na_v1.4$ channels at the measured V_{rest} of approximately −50 mV. It is important to note that this up-regulation of basal VGSC activity is not specific for this exact value of V_{rest}. Window currents are similarly up-regulated by a factor of two to four in the whole range of physiologically sensible resting membrane potentials, i.e., between −50 and −90 mV. Therefore, while it may be likely that the measured value of V_{rest} is specific to the particular genetic background of these mice or the investigated muscle type, and indeed estimates of V_{rest} vary widely in literature (Head, 1993; Woods et al., 2005), the end effect of significantly higher basal VGSC activity should hold in the majority of cases.

These observations of longer open dwell times and greater basal activity of $Na_v1.4$s produce a good ground for explaining the observed approximately twofold increase in $[Na^+]$ under the sarcolemma of *mdx*^{5cv} fibers. Indeed, combining the 1.5 factor of longer open dwell times with the 2× higher frequency of openings at the V_{rest} of −50 mV, or even 3× at V_{rest} of −75 mV, we arrive at ∼3× or even 5× greater forcing of Na^+ entry by the $Na_v1.4$ channels at the corresponding resting membrane potentials, sufficient to sustain elevated $[Na^+]_i$ even in view of an ∼20% smaller driving force for Na^+ in *mdx* cells at rest. Such an increase is in good agreement with measurements reported elsewhere (Yeung et al., 2003), performed using Na^+ green fluorescence. Thus, it can be argued that changes in $Na_v1.4$ gating properties significantly affect the Na^+ balance in FBD muscle fibers, producing an important long-term effect even in nonexercised muscle.

It is interesting to note that no significant changes in Na^+ currents in *mdx*-deficient EDL fibers were reported by others (Mathes et al., 1991). One apparent difference that could account for this discrepancy is the different type of muscle investigated; however there are other avenues to investigate. In our study, mice were age matched (12–16 wk old), corresponding, in *mdx*^{5cv} mice, to the phase of slow chronic disease after full recovery from the initial massive necrosis episode. Using mice of that age may have been an important factor, maximizing the differences between control and *mdx*-deficient fibers. Moreover, careful examination of the figure in Mathes et al. suggests that these authors, similarly to us, may have been faced with significant patch-to-patch variability, possibly masking the difference between control and *mdx* fibers, with steady-state inactivation thresholds being slightly, but not significantly, shifted toward positive potentials, and τ_i's being slightly longer in *mdx* cells.

Deregulation, by the absence of dystrophin, of $Na_v1.4$ activity leading to Na^+ overload is likely connected with multiple other changes reported in *mdx* fibers. Thus, the reduced expression levels of $Na_v1.4$ channels might be explained by a compensatory mechanism down-regulating, via the E box motif, their expression in response to the increase in Na^+ influx via VGSCs. This motif plays a critical role in regulating $Na_v1.4$ expression through binding to a complex of proteins (Kraner et al., 1998). Another compensatory mechanism may be causing an increased activity and expression of the Na^+/K^+ATPase in order to counteract the $[Na^+]_i$ overload in *mdx* muscle (Dunn et al., 1995). Alternatively, an elevated Na^+ influx in skeletal muscle as well as in neurons, might lead directly either to caspase-3 activation, or to a subsequent Ca^{2+} entry, due to the Na^+/Ca^{2+} exchanger, which in its reverse mode induces Ca^{2+}-dependent cell death (Banasiak et al., 2004). Another possibility is that other proteins might be involved in skeletal muscle dysfunction. For example, the β-subunit of the channel, thought to have a regulatory function, may be altered by the absence of dystrophin. Such a dysfunction of the β-subunit could be responsible for the decreased inactivation rate observed in *mdx*^{5cv} fibers. Work is in progress to determine events downstream of Na^+ overload leading to increased cell death in *mdx*^{5cv} fibers.

Downloaded from http://rupress.org/jgp/article-pdf/132/2/199/1785739/jgp_200810024.pdf by guest on 09 February 2026

We thank M. Schaub for providing anti–α1-syntrophin antibodies, and F.X. Boittin and O.M. Dorchies for their suggestions and advice. We are grateful to J.L. Bény (University of Geneva, Geneva, Switzerland) for letting us use some of his equipment.

This study was supported by grants from the Swiss National Science Foundation (grant 3100A0-109981), the Swiss Foundation for Research on Muscular Diseases, and the Association Française contre les Myopathies.

Olaf S. Andersen served as editor.

Submitted: 10 April 2008
Accepted: 25 June 2008

REFERENCES

Allen, D. 2004. Skeletal muscle function: role of ionic changes in fatigue, damage and disease. *Clin. Exp. Pharmacol. Physiol.* 31:485–493.

Banasiak, K.J., O. Burenkova, and G.G. Haddad. 2004. Activation of voltage-sensitive sodium channels during oxygen deprivation leads to apoptotic neuronal death. *Neuroscience.* 126:31–44.

Blake, D.J., A. Weir, S.E. Newey, and K.E. Davies. 2002. Function and genetics of dystrophin and dystrophin-related proteins in muscle. *Physiol. Rev.* 82:291–329.

Bloch, R.J., Y. Capetanaki, A. O'Neill, P. Reed, M.W. Williams, W.G. Resneck, N.C. Porter, and J.A. Ursitti. 2002. Costameres: repeating structures at the sarcolemma of skeletal muscle. *Clin. Orthop. Relat. Res.* 403:203–210.

Boittin, F.-X., O. Petermann, C. Hirn, P. Mittaud, O.M. Dorchies, E. Roulet, and U.T. Ruegg. 2006. Ca^{2+}-independent phospholipase A2 enhances store-operated Ca^{2+} entry in dystrophic skeletal muscle fibers. *J. Cell Sci.* 119:3733–3742.

Catterall, W.A. 1988. Structure and function of voltage-sensitive ion channels. *Science.* 242:50–61.

Constantinides, C.D., J.S. Gillen, F.E. Boada, M.G. Pomper, and P.A. Bottomley. 2000. Human skeletal muscle: sodium MR imaging and quantification-potential applications in exercise and disease. *Radiology.* 216:559–568.

Dunn, J., N. Bannister, G.J. Kemp, and S.J. Publicover. 1993. Sodium is elevated in mdx muscles: ionic interactions in dystrophic cells. *J. Neurol. Sci.* 114:76–80.

Dunn, J.F., K.A. Burton, and M.J. Dauncey. 1995. Ouabain sensitive Na^+/K^+-ATPase content is elevated in mdx mice: implications for the regulation of ions in dystrophic muscle. *J. Neurol. Sci.* 133:11–15.

Fong, P.Y., P.R. Turner, W.F. Denetclaw, and R.A. Steinhardt. 1990. Increased activity of calcium leak channels in myotubes of Duchenne human and *mdx* mouse origin. *Science.* 250:673–676.

Gailly, P. 2002. New aspects of calcium signaling in skeletal muscle cells: implications in Duchenne muscular dystrophy. *Biochim. Biophys. Acta.* 1600:38–44.

Gavillet, B., J.-S. Rougier, A.A. Domenighetti, R. Behar, C. Boixel, P. Ruchat, H.-A. Lehr, T. Pedrazzini, and H. Abriel. 2006. Cardiac sodium channel Nav1.5 is regulated by a multiprotein complex composed of syntrophins and dystrophin. *Circ. Res.* 99:407–414.

Gee, S.H., R. Madhavan, S.R. Levinson, J.H. Caldwell, R. Sealock, and S.C. Froehner. 1998. Interaction of muscle and brain sodium channels with multiple members of the syntrophin family of dystrophin-associated proteins. *J. Neurosci.* 18:128–137.

Goldin, A.L. 2001. Resurgence of sodium channel research. *Annu. Rev. Physiol.* 63:871–894.

Head, S.I. 1993. Membrane potential, resting calcium and calcium transients in isolated muscle fibres from normal and dystrophic mice. *J. Physiol.*. 469:11–19.

Hodgkin, A.L., and A.F. Huxley. 1952. A quantitative description of membrane current and its application to conduction and excitation in nerve. *J. Physiol.* 117:500–544.

Koenig, M., A.P. Monaco, and L.M. Kunkel. 1988. The complete sequence of dystrophin predicts a rod-shaped cytoskeletal protein. *Cell.* 53:219–226.

Koike, T., S. Tanaka, T. Oda, and T. Ninomiya. 2000. Sodium overload through voltage-dependent Na^+ channels induces necrosis and apoptosis of rat superior cervical ganglion cells in vitro. *Brain Res. Bull.* 51:345–355.

Kraner, S.D., M.M. Rich, R.G. Kallen, and R.L. Barchi. 1998. Two E-Boxes are the focal point of muscle-specific skeletal muscle type 1 Na^+ channel gene expression. *J. Biol. Chem.* 273:11327–11334.

Mathes, C., F. Bezanilla, and R.E. Weiss. 1991. Sodium current and membrane potential in EDL muscle fibers from normal and dystrophic (mdx) mice. *Am. J. Physiol. Cell Physiol.* 261:C718–C725.

Ribaux, P., F. Bleicher, M.L. Couble, J. Amsellem, S.A. Cohen, C. Berthier, and S. Blaineau. 2001. Voltage-gated sodium channel (SkM1) content in dystrophin-deficient muscle. *Pflugers Arch.* 441:746–755.

Ritchie, J., and R. Rogart. 1977. The binding of saxitoxin and tetrodotoxin to excitable tissue. *Rev. Physiol. Biochem. Pharmacol.* 79:1–50.

Ruegg, U.T., V. Nicolas-Metral, C. Challet, K. Bernard-Helary, O.M. Dorchies, S. Wagner, and T.M. Buetler. 2002. Pharmacological control of cellular calcium handling in dystrophic skeletal muscle. *Neuromuscul. Disord.* 12:S155–S161.

Ulbricht, W. 2005. Sodium channel inactivation: molecular determinants and modulation. *Physiol. Rev.* 85:1271–1301.

Williams, M.W., and R.J. Bloch. 1999a. Differential distribution of dystrophin and β-spectrin at the sarcolemma of fast twitch skeletal muscle fibers. *J. Muscle Res. Cell Motil.* 20:383–393.

Williams, M.W., and R.J. Bloch. 1999b. Extensive but coordinated reorganization of the membrane skeleton in myofibers of dystrophic (mdx) mice. *J. Cell Biol.* 144:1259–1270.

Woods, C.E., D. Novo, M. DiFranco, J. Capote, and J.L. Vergara. 2005. Propagation in the transverse tubular system and voltage dependence of calcium release in normal and mdx muscle fibres. *J Physiol.* 568:867–880.

Yeung, E.W., S.I. Head, and D.G. Allen. 2003. Gadolinium reduces short-term stretch-induced muscle damage in isolated mdx mouse muscle fibres. *J. Physiol.* 552:449–458.

Downloaded from http://rupress.org/jgp/article-pdf/132/2/199/1785739/jgp_200810024.pdf by guest on 09 February 2026